Proc. Nat. Acad. Sci. USA
Vol. 73, No. 3, pp. 823–827, March 1976
Biophysics

Inactivation of catalase monolayers by irradiation with 100 keV electrons

(model membranes/electron microscopy/dosimetry/radiation damage)

M. HAHN, J. SEREDYNSKI, AND W. BAUMEISTER

Institut für Biophysik und Elektronenmikroskopie der Universität Düsseldorf, Moorenstr. 5, D-4000 Düsseldorf 1, West Germany

Communicated by A. Frey-Wyssling, December 29, 1975

ABSTRACT **A catalase monolayer adsorbed on a layer of arachidic acid deposited on a solid support was irradiated with 100 keV electrons simulating the conditions of electron microscopic imaging. Effective doses were calculated taking into account the angular and energy distribution of backscattered electrons. Enzymatic inactivation was chosen as the criterion for damage and was monitored by a rapid and quantifiable but nevertheless sensitive assay. Dose–response curves revealed that inactivation is a one-hit–multiple-target phenomenon, which is consistent with biochemical evidence for a cooperative function of subunits. The experimentally determined target size coincides fairly well with both calculated cross sections for inelastic interactions based on the atomic composition of catalase and with calculated cross sections for ionizing events based on the chemical bonds involved. This legitimates both types of calculations even for complex biomolecules.**

Macromolecules and supramolecular assemblies are subject to substantial structural alterations when exposed to the unfavorable conditions in the electron microscope. Theoretical considerations (1) as well as experimental investigations (for review see ref. 2) led to the suspicion that radiation-induced deteriorations of the molecular structure might fundamentally limit the resolution to which reliable structural information can be obtained. The degree of structural alteration is a function of the radiation sensitivity of the specimen under investigation and of the electron dose deposited on it, which in turn is defined by the wanted resolution (3, 4). Subtle structural alterations which can be neglected at moderate resolution levels become increasingly important with increasing resolution.

The complexity of the phenomena associated with radiation damage of proteins or biomolecules in general made it impossible to formulate inductively a universal theory of the damaging process (for reviews see refs. 5–7) which could define or even predict the kind and degree of structural alterations following the fairly well understood physical interaction between the beam electrons and the specimen atoms. For essentially the same reason it is impossible to trace back on a theoretical basis to the original undisturbed structure of a protein from micrographs with manifest deteriorations.

To evaluate realistic perspectives for "molecular microscopy" it seems necessary to measure quantitatively the electron doses causing distinct structural deterioration in various molecular species of biological relevance and under experimental conditions simulating the hazards of electron microscopical imaging. Hitherto, radiation damage was often measured by determining the dose that caused fading of distinct spots of the electron diffraction pattern. Unfortunately, this method is confined to crystalline specimens and, moreover, the situation of a molecule in a crystal need not necessarily reflect its reaction to ionizing radiation in a noncrystalline state. Organized monolayer systems assembled in a controlled sequence at the water–air interface and deposited upon solid supports offer suitably thin and defined model systems, which are comparable to not necessarily crystalline, real electron microscopic specimens.

To circumvent the difficulties involved in experimentally simulating the "single-transmission" situation of electron microscopy we here describe a dosimetry taking into account the electrons backscattered from the solid support. As a criterion for damage we have chosen the loss of enzymatic activity, though it cannot yet directly be ascribed to distinct structural alterations within a given protein. Nevertheless we presume enzyme inactivation to be a sensitive and quantifiable indicator reflecting a relatively definable degree of structural change and, moreover, being a prominent though comparatively early point in the destructive process that may finally reach a "steady state" (8). In this context we report on a rapid semiquantitative but nevertheless sensitive assay to monitor inactivation of catalase, which is of considerable advantage for testing the efficiency of the numerous potential radiation protectants. The design of protective systems appears to be a third promising approach to "nondestructive" molecular microscopy besides minimal beam exposure techniques (9) and the sophisticated utilization of structural redundancies (10).

MATERIALS AND METHODS

Monolayer Formation. Catalase monolayers were formed by adsorption onto a lipid monolayer, similar to the procedure described by Fromherz (11, 12). Arachidic acid (Fluka, Switzerland) is spread at the water–air interface of a Langmuir trough and compressed until a film pressure of 200 μN/cm is reached. By means of a motor-driven transfer mechanism and a constant pressure device (13) the arachidic acid layers are deposited on an electro-gilded brass plate, such that the polar groups are in contact with the gold surface and the hydrophobic parts extend outwards. Beef liver catalase (hydrogen-peroxide:hydrogen-peroxide oxidoreductase, EC 1.11.1.6) from Boehringer (Germany) is allowed to adsorb to the arachidic-acid-coated plate from solution (0.05 M sodium phosphate buffer, pH 6.8, 0.3 g protein per liter of buffer solution, 298 K) for 20 min to ensure a closely packed monolayer. To remove loosely bound protein the plates are washed twice in the same buffer solution. Homogeneity of the layers was checked by electron microscopic observation of layers negatively stained with potassium phosphotungstate.

Irradiation. The coated plates were inserted into a device that allowed us to shift them under a stationary metal frame in the image plane of an electron microscope (Siemens Elm-

Abbreviations: b.e., backscattered electrons; p.e., primary electrons.

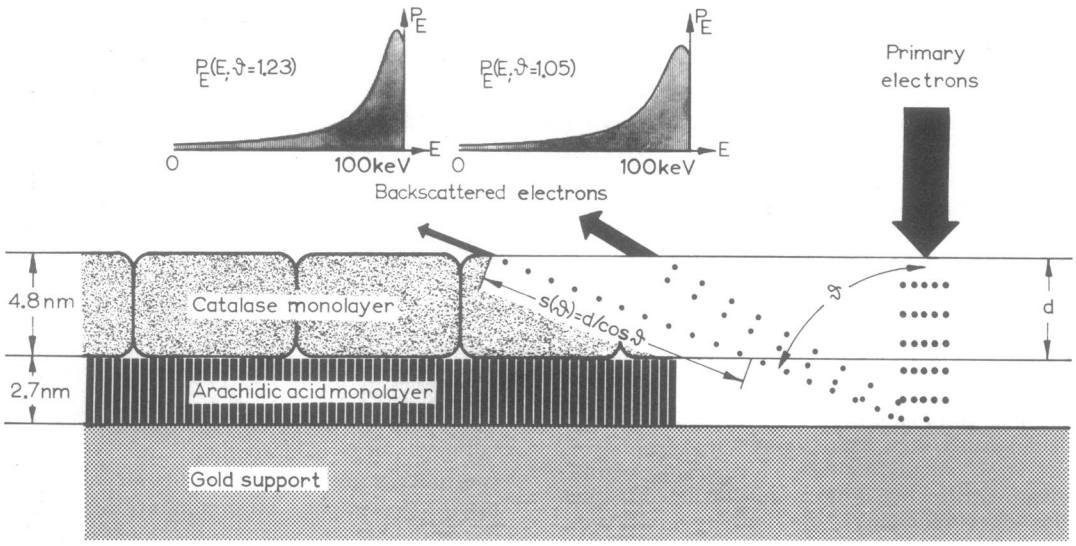

FIG. 1. Geometry of irradiation of monolayers on a solid support. The number of dotted lines symbolizes the relation numbers of b.e. to p.e.; the distance between the dots symbolizes the relative mean free path between damaging events.

iskop Ia). Successively the plates were adjusted under the window in the frame to allow the electron beam to irradiate only one half of each plate, so keeping a nonirradiated part of otherwise equal treatment for comparison. The incident current density was obtained by measuring the total current I_m spread over a homogenously illuminated circular patch of diameter b. Regarding the efficiency $y < 1$ (14) of the built-in image-current meter, which uses the insulated final screen as electron collector the incident current density was $j = 4\, I_m/\pi b^2 y$. Choosing $j \approx 5{\cdot}10^{-8}$ A cm^{-2} excluded any risk of temperature rise above room temperature (295 K). Before irradiation the gun was allowed to reach a steady state, i.e., to deliver a constant current I_m. The vacuum was always below $2{\cdot}10^{-5}$ torr (2.7 mPa). 100 kV accelerating voltage was chosen to minimize multiple scattering in the specimen and to achieve similarity to most of today's high resolution electron microscopic work.

Dosimetry on Solid Supports. The assay described above demands the deposition of the specimen on the surface of a solid plate that is far too thick to be penetrated by the 100 keV beam electrons. To compare the effective doses acting on the thin ($\leq 10^{-6}$ g cm^{-2}) specimen resting on the plate with the doses collected by the same specimen in transmission electron microscopy on supports of approximately $3{\cdot}10^{-7}$ g cm^{-2}, the dose due to backscattered electrons (b.e.) has to be accounted for.

If $\sigma_k(E)$ is the cross section for an interaction of kind k, dependent on the electron kinetic energy E, and for every incident primary electron (p.e.), we count η b.e. (η = backscattering yield factor) with normalized probability distributions $P_\vartheta(\vartheta) \sin\vartheta\, d\vartheta\, d\varphi$ over the angle ϑ and $P_E(E/E_b;\, \vartheta)\, d(E/E_b)$ over the relative energy E/E_b we can define a factor

$$f_k = q_{k\,\mathrm{eff}}/q_{kn} > 1 \qquad [1]$$

converting the nominal doses q_{kn} applied to the specimens into effective doses $q_{k\,\mathrm{eff}}$ yielding the same effects in case of one-way transmission of p.e. For normally incident p.e., P_ϑ is independent of azimuth φ; therefore, we set $d\Omega = 2\pi \sin\vartheta\, d\vartheta$ and obtain for E_b = energy of p.e. (Fig. 1).

$$f_k = 1 + \frac{\eta}{\sigma_k(E_b)} \int_0^{\pi/2} \int_0^{E_0} \sigma_k(E) P_E(E/E_b;\, \vartheta) \frac{P_\vartheta(\vartheta)}{\cos\vartheta} dE\, d\Omega. \qquad [2]$$

For numerical evaluation of Eq. 2 we fitted experimental values for P_ϑ (15) to a Lambert distribution and for P_E (15, 16) to a generalized Lorentzian (17). η (Au; 100 keV) = 0.513 is also known from measurements (18).

To account for the loss of energy exchange capability of electrons at very low energies (19) and to cut off the influence of "true" secondary electrons (20)*, i.e., electrons liberated in ionizing processes, we use an effective charge factor

$$\kappa(E) = 1 - \exp(-125\beta). \qquad [3]$$

This is reasonable, because their penetration depth is smaller than the thickness of the arachidic acid monolayer (2.7 nm) separating the catalase monolayer from the gold surface, and the secondary electron yield from the intermediate layer itself is small compared to the yield from the bulk gold (21).

Assuming inelastic scattering responsible for damage, we evaluated Eq. 2 with a cross-section formula (22)

$$\sigma_{in}(E) = \frac{3}{4} \frac{\lambda_c^2 (\ln B - \beta^2)}{\pi\beta^2} \sum_i \sqrt{Z_i} \qquad [4]$$

with

β = electron velocity/velocity of light
λ_c = Compton wavelength = $2.425 \cdot 10^{-3}$ nm
$B = \frac{2E_0\beta}{E_1}\left[\frac{E(2 + E/E_0)}{E_0(1 - \beta^2)}\right]^{1/2}$

and

E_1 = 37 eV = mean inelastic energy loss per event
E_0 = 511.3 keV = rest energy of the electron
Z = atomic number

For comparison, we also used gross-ionization cross sections (23)

$$\sigma_{g.i.} = \frac{\lambda_c^2 M_i^2}{\pi\beta^2} \left\{ \ln \frac{c_i E_0 \beta^2}{2(1 - \beta^2)} - \beta^2 \right\} \qquad [5]$$

with relative oscillator strength factors M_i^2 and voltage coef-

* Because electrons are indistinguishable from each other, this discrimination is only justified by the shape of the energy distribution.

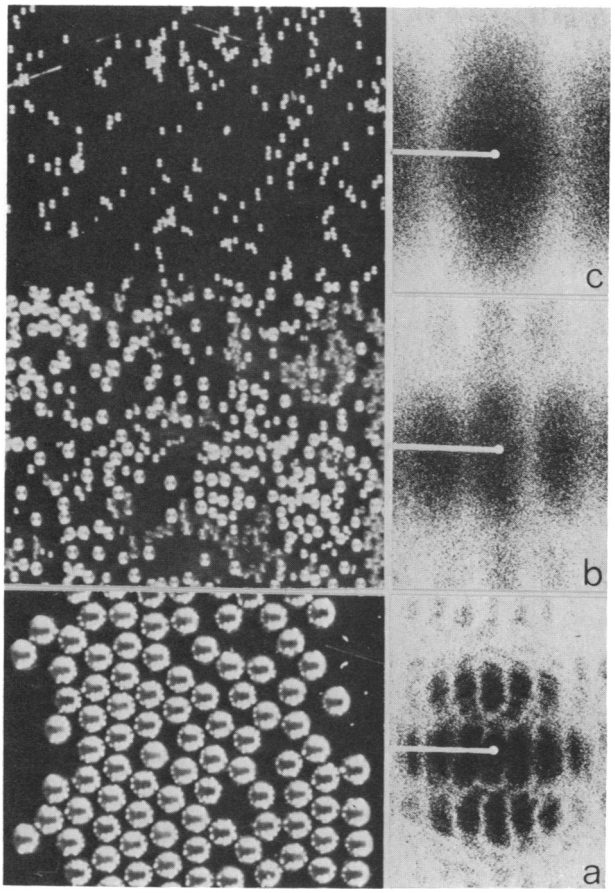

FIG. 2. Photographs and diffractograms of: (a) Steel balls of 1/32 inch = 0.794 mm diameter (standard). (b) Nonirradiated part of plate shown in Fig. 3b. Mean bubble diameter 0.427 mm. (c) Irradiated part of plate shown in Fig. 3b. Mean bubble diameter 0.213 mm.

ficients c_i for different bond types taken from measurements on hydrocarbon gases (24):

Symbol	Bond type	M_i^2	c_i·eV
a	C—H	1.07	0.134
b	σ(C—C)	2.5	0.0676
c	π(C—C)	0.4	0.107
	C_6H_6-rings	24.4	0.102

With $\sigma_k(E) = \sigma_{in}(E)\,\kappa^2(E)$ we calculated $f_{in} = 1 + 1.7$ and for $\sigma_k(E) = \sigma_{g.i.}(E)\,\kappa^2(E)$ we obtained $f_{g.i.} = 1 + 1.6$.

Enzyme Activity Assay. A rapid semiquantitative assay has been used for the determination of enzymic activity, measuring the rate of oxygen generation in diluted H_2O_2. It is a certain advantage of this method that it easily avoids errors due to different kinetics in irradiated and nonirradiated samples which are due to changes in the substrate concentration in the microenvironment of the bound enzymes. The influence of different kinetics has always to be considered carefully, since it significantly influences the shape of dose–response curves. After irradiation the plates were immersed in a solution of 0.15% H_2O_2 in water (287 K). Photographs of the appearing oxygen bubbles were taken at intervals of 7 sec. The very first photographs showed no indication of diffusion-limited turnover rates on both halves of the plates. The mean diameters of the oxygen bubbles were determined on light-optical diffractograms of these photos by comparing the size of intensity lobes in the power spectrum of bubble images with the lobes from steel balls of known diameter.

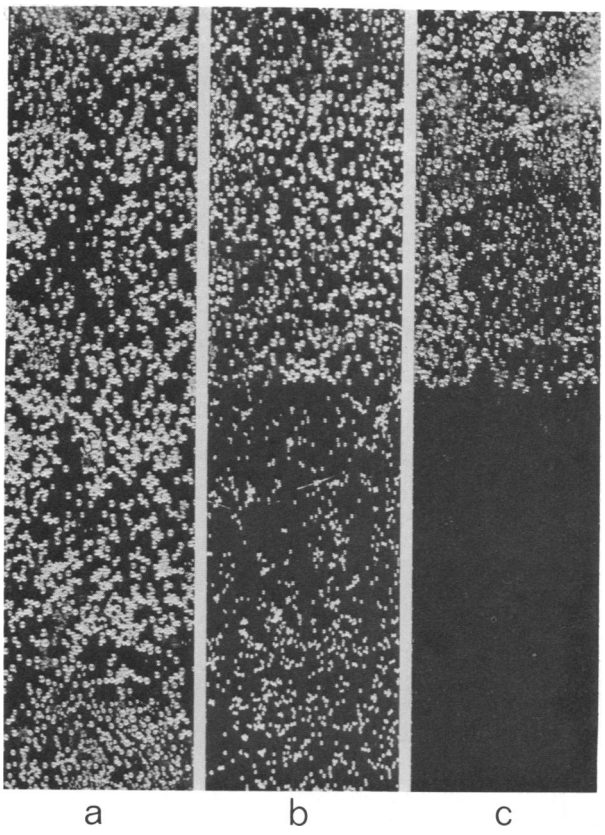

FIG. 3. Photographs of catalase-coated plates 15 sec after immersion in 0.15% H_2O_2. Upper halves were not irradiated; lower halves were irradiated with: (a) 1.3; (b) 2.8; (c) 4.1 p.e./nm^2.

The oxygen content of the mean bubble was calculated considering the noticeable pressure rise due to surface tension. The mean number of bubbles per unit area was determined by counting them in test fields (Figs. 2 and 3).

RESULTS AND DISCUSSION

Enzymatic activity in the monolayer

Assuming a maximum number of $1.56 \cdot 10^{12}$ catalase molecules per cm^2 (closely packed ideal monolayer) the activity in the nonirradiated halves of the plates is approximately 1/6 of the specific activity as measured in a solution. This discrepancy is obviously mainly due to the rate-limiting low substrate concentration in our assay (to ease photographic recording) and nonoptimum pH and temperature conditions, and far less to enzyme denaturation during adsorption and dehydration or deviations from ideality in monolayer structure.

Vacuum effects

It seems remarkable that the exposure of catalase monolayers to vacua below 10^{-5} torr (1.3 mPa) does not significantly alter the enzymatic activity as compared to layers kept in a wet state. Dehydration of catalase monolayers under microscopic vacuum conditions is obviously not as harmful for single molecules as it is for supramolecular assemblies. It is well known from crystallographic studies of proteins (25) that the crystals shrink upon dehydration in a discontinuous manner, which is accompanied by profound changes in the diffraction pattern. Catalase crystals are observed to shrink by about 40% in length and 15% in width on air drying (26) and electron diffraction studies comparing

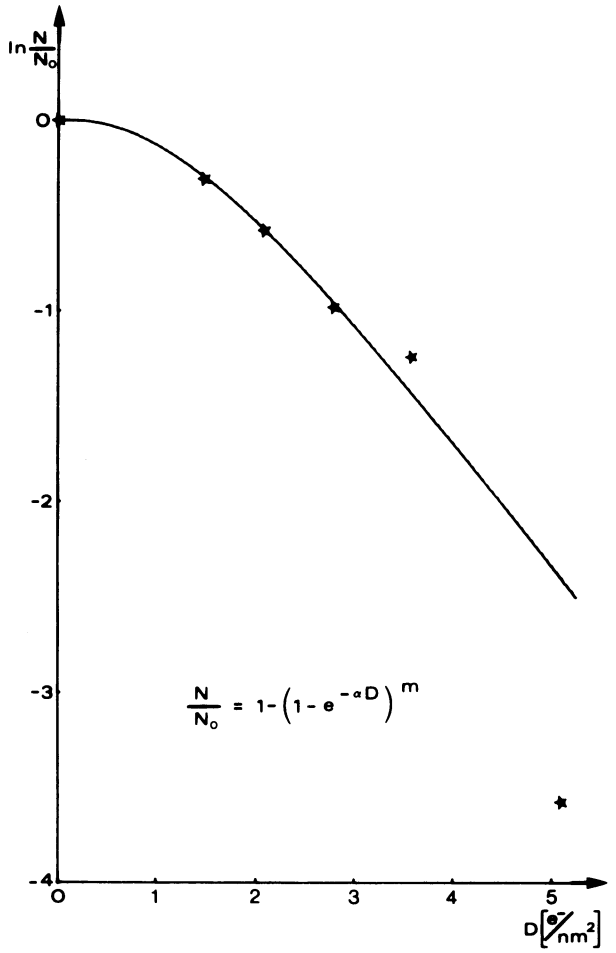

FIG. 4. Dose–response of catalase activity. D = applied dose in electrons per nm^2; α = target area; m = number of targets; N/N_0 = activity in irradiated area/activity in nonirradiated area. Graph computed for $m = 3$.

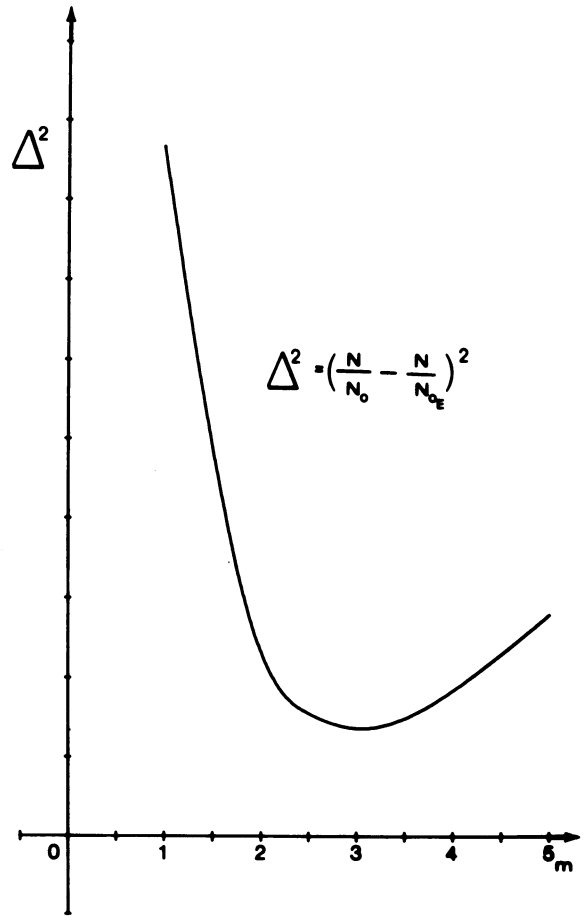

FIG. 5. Mean square error Δ^2 for different numbers of targets (m). N/N_{0E} = fractional activity as measured.

dry and wet catalase crystal indicate that drying seriously disorders the crystal (27). The fact that vacuum drying does not affect the enzymic activity of catalase suggests that fading of the low angle intensities of the electron diffraction pattern reflects only disorder of the crystal and not damage to individual molecules. It seems remarkable in this context that this retention of activity is valid for unstained but not for negatively stained catalase (28).

Inactivation

On the plates a decrease of enzymic activity is already detectable at doses as low as 1.5 e$^-$/nm^2 and inactivation is almost complete at 5 e$^-$/nm^2. Plotting a dose–response curve for catalase inactivation (Fig. 4) reveals a shape which according to the stochastics of radiative action can be ascribed to multi-hit and/or to multiple-target processes. Our experimental data are by far best fitted by a three-target–one-hit curve (Figs. 4 and 5) for targets of 0.67 ± 0.035 nm^2 each. As catalase consists of four subunits each having one hematin group as an active site, this implies that three of the active groups must be destroyed before the enzyme loses its activity. This agrees fairly well with biochemical evidence that at least two active sites might need to act cooperatively to bring about the catalytic action (29, 30). Eq. **2** yielded σ_{in} (100 keV) = 2.48 nm^2 for a catalase molecule of the atomic composition 16036 H, 10504 C, 2960 N, 3012 O, 56 S, and 4 Fe (31), while Eq. **5**, assuming 1.64 ion pairs per cluster (32), yielded a cross section σ_{cl} for ion-cluster generation in a catalase molecule represented by 15020 *a*-, 15532 *b*-, 2856 *c*-bonds, and 224 C_6H_6-rings of σ_{cl} = 2.07 nm^2.

Earlier measurements

Comparison with early measurements (33) of inactivation cross-sections on dry catalase by 3.8 MeV deuterons reveals that their approximately 80-fold higher linear energy transfer is the cause for the strong temperature dependence and exaggerated size of these cross sections. Application of the thermal-spike model (34) leads to the same inactivation temperature of 432 K for the cross sections 14.2, 24.5, and 42 nm^2 given in Table 1 of ref. 33. Also delta-ray correction using the theory of Butts and Katz (35) stepped up the cross sections reported here to over 10 nm^2 for 3.8 MeV deuterons.

Conclusions

From the molecular volume $v_M \approx 307$ nm^3 follows a mean free path λ_{in} = 124 nm for inelastic events and of λ_{cl} = 149 nm for ion cluster generation. This means that damaging events in three volumes of 83 nm^3 and 100 nm^3, respectively, inactivate the molecule. Not only the fairly good coincidence of total cross sections added up from single atoms with those added up for single bonds, but also the coincidence of measured inactivation volumes with the volume of the catalase subunits is remarkable. The result of roughly one inelastic event's rendering a subunit of approximately 60,000 molecular weight inactive implies that, regardless of where the

primary energy is released within the subunit, intramolecular energy transfer is efficient enough to reach critical sites. Energy dissipation without manifest effects seems to be rather unlikely.

Moreover, it is evident that primary energy exchange processes are sufficiently confined to allow summing up of interaction cross sections measured on small constituents to valuable data even for large, complex molecules.

We thank Mrs. Ludolph and Miss Kikhoefer for technical assistance. This work was supported by the Deutsche Forschungsgemeinschaft, Grant Ru 5/17.

1. Breedlove, J. R. & Trammell, G. T. (1970) *Science* **170,** 1310–1313.
2. Glaeser, R. M. (1975) in *Physical Aspects of Electron Microscopy and Microbeam Analysis,* eds. Siegel, B. M. & Beaman, D. R. (John Wiley & Sons, New York), pp. 205–229.
3. Glaeser, R. M. (1971) *J. Ultrastruct. Res.* **36,** 466–482.
4. Baumeister, W. & Hahn, M. (1975) *Hoppe-Seyler's Z. Physiol. Chem.* **356,** 1313–1316.
5. Augenstine, L. G. (1962) in *Advances in Enzymology and Related Subjects of Biochemistry,* ed. Nord, F. F. (Interscience Publishers, New York), Vol. 24, pp. 359–413.
6. Luse, R. A. (1964) *Radiat. Res. Suppl.* **4,** 192–212.
7. Dertinger, H. & Jung, H. (1970) *Molecular Radiation Biology* (Springer-Verlag, New York-Heidelberg-Berlin, Science Library), Vol. 12.
8. Stenn, K. & Bahr, G. F. (1970) *J. Ultrastruct. Res.* **31,** 526–550.
9. Williams, R. C. & Fischer, H. W. (1970) *J. Mol. Biol.* **52,** 121–123.
10. Unwin, P. N. T. & Henderson, R. (1975) *J. Mol. Biol.* **94,** 425–440.
11. Fromherz, P. (1969) Ph.D. Dissertation, Universität Marburg.
12. Fromherz, P. (1971) *Biochim. Biophys. Acta* **225,** 382–386.
13. Baumeister, W. & Hahn, M. (1975) in *Progress in Surface and Membrane Science,* eds. Danielli, F. F. & Cadenhead, D. A. (Academic Press, New York), in press.
14. Grubb, D. T. (1971) *J. Phys. E: Sci. Instr.* **4,** 222–224.
15. Kanter, H. (1957) *Ann. Phys.* **20,** 144–166.
16. Kulenkampff, H. & Spyra, W. (1954) *Z. Phys.* **137,** 416–425.
17. Lenz, F. (1950) *Z. Angew. Phys.* **2,** 337–340.
18. Drescher, H., Krefting, E. R., Reimer, L. & Seidel, H. (1974) *Z. Naturforsch. Teil A* **29,** 833–837.
19. Barkas, H. (1963) *Nuclear Research Emulsion* (Academic Press, New York), Vol. I.
20. Kim, Y.-K. (1975) *Radiat. Res.* **61,** 21–35.
21. Kanter, H. (1961) *Phys. Rev.* **121,** 681–684.
22. Isaacson, M. S. (1975) in *Principles and Techniques of Electron Microscopy,* ed. Hayat, M. A. (Van Nostrand Reinhold Co., New York), Vol. 6, in press.
23. Schram, B. L., De Heer, F. J., van der Wiel, M. J. & Kistemaker, J. (1965) *Physica* **31,** 94–112.
24. Schram, B. L., van der Wiel, M. J., De Heer, F. J. & Moustafa, H. R. (1966) *J. Chem. Phys.* **44,** 49–54.
25. Huxley, H. E. & Kendrew, J. C. (1953) *Acta Crystallogr.* **6,** 76–80.
26. Longley, W. (1967) *J. Mol. Biol.* **30,** 323–327.
27. Matricardi, V. R., Moretz, R. C. & Parsons, D. F. (1972) *Science* **177,** 268–270.
28. Baumeister, W. & Hahn, M. (1975) *Naturwissenschaften* **62,** 36.
29. Deisseroth, A. B. & Dounce, A. L. (1967) *Arch. Biochem. Biophys.* **120,** 671–692.
30. Deisseroth, A. B. & Dounce, A. L. (1969) *Arch. Biochem. Biophys.* **131,** 39–48.
31. Schroeder, W. A., Shelton, J. R., Shelton, J. B., Robberson, B. & Apell, G. (1969) *Arch. Biochem. Biophys.* **131,** 653–655.
32. Ore, A. & Larsen, A. (1964) *Radiat. Res.* **21,** 331–338.
33. Setlow, R. B. (1952) *Proc. Nat. Acad. Sci. USA* **38,** 166–172.
34. Ingalls, R. B., Spiegler, P. & Norman, A. (1964) *J. Chem. Phys.* **41,** 837.
35. Butts, J. J. & Katz, R. (1967) *Radiat. Res.* **30,** 855.